May 7, 2015

Supplementary Information for Truex et al., submitted to PRL

Materials and Methods:

The ideal comparison would be to study the same DNA hairpins used in the force experiments. However, that is not yet possible because their high stability and low transition frequency make them inaccessible to single molecule FRET measurements, which require folding and unfolding times on the millisecond time scale or less for acquiring data before fluorophore bleaching at the necessarily high illumination intensities terminates the photon trajectories.

Synthesis, labeling with Alexa Fluor dyes, and purification of model DNA hairpin. A biotinylated version of the DNA hairpin sequence [5'-AACC(T_{21})GGTT-3'] was labeled with a donor/acceptor fluorescent dye pair for single molecule FRET measurements. To help avoid artifacts arising from surface immobilization, a 10-deoxythymidine linker was included to add separation of the hairpin from both the biotin group and the surface (Fig. 2 shows the dye-labeled DNA hairpin). The modified DNA hairpin 5'- BiotinT-(T_{10})-AACC-iAmMC6T-(T_{20})-GGTT-3ThioMC3-3', where iAmMC6T and 3ThioMC3 denote internal amino modifier C6-dT and 3' thiol modifier C3 S-S, respectively, was synthesized, purified by reverse-phase high pressure liquid chromatography, and verified by mass spectrometry (12923 Da) by Integrated DNA Technologies.

200 μg of the modified DNA (10mg/ml) was mixed with 112.5 μL of 0.1 M $Na_2B_4O_7$, pH 8.5 and reacted with 260 μg of Alexa Fluor 488 NHS ester (Life Technologies) dissolved in 17.5 μL DMSO for 6 hr at room temperature. The reaction was terminated by the addition of 15 μL 3 M sodium acetate, pH 5.2 and 3 volumes of ethanol. The mixture was frozen in dry ice/ethanol bath for 30 min, thawed and spun in an Eppendorf centrifuge at maximum speed (4 °C) for 15 min. The DNA pellet was rinsed twice with ethanol, dried, dissolved in 5 mL 25 mM Tris-HCl, pH 8 and subjected to anion-exchange chromatography (Mono Q 5x5 GL, GE Healthcare) using a 0 to 1 M linear NaCl gradient in the same buffer to separate the Alexa Fluor 488-labeled DNA from unlabeled DNA. Peak fractions of the labeled DNA were combined and concentrated using Amicon centrifugal filters (Merck Millipore Ltd.). The DNA was incubated in a total volume of 150 μL 50 mM Tris-HCl, pH 7.5 containing 1.5 mM TCEP [Tris(2-carboxy-ethyl)phosphine] hydrochloride (Sigma Aldrich) for 2 hr to reduce the 3'-thiols and then reacted with 200 μg Alexa Fluor 594 C_5 maleimide (Life Technologies) dissolved in 10 μL DMSO for an additional 2 hr. The reaction was terminated by the addition of 2-mercaptoethanol to a final concentration of 10 mM and incubation for 10 min. The excess dye was removed by size-exclusion chromatography on Superdex-30 (1 x 30 cm, GE Healthcare) at a flow rate of 0.5 ml/min in 0.5x phosphate buffered saline at room temperature. Peak fractions were concentrated and stored in aliquots in -20 °C.

The purified fraction that had equal concentrations of the two dyes, as determined by bulk UV absorption, was used for single molecule spectroscopy. Bulk fluorescence spectroscopy confirmed salt dependent FRET transfer between the two dyes.

Thermal unfolding.A thermal unfolding curve was determined by measuring the optical density at 260 nm for the unmodified DNA sequence [5'-AACC(T_{21})GGTT-3'] (Integrated DNA Technologies Inc.) without biotin, linkers, or dyes (Cary 100 UV-VIS spectrophotometer, Agilent Technologies). The solution contained 3 μM DNA, 500 mM NaCl, 250 μM EDTA, and 2.5 mM TRIS-HCl (pH 8.0). The data was fit with a two-state model assuming linear pre- and post-transition baselines. Since the lower baseline was not observed, it was assumed to be parallel to the upper baseline. Data and baselines are shown in FIG. S1A, and the unfolded fraction calculated from the two-state fit is shown in FIG. S1B.

Single molecule spectroscopy. Single molecule measurements were carried out with a confocal microscope system (MicroTime200, Picoquant) equipped with an oil-immersion objective (PlanApo, NA 1.4, × 100, Olympus). The continuous-wave mode of a dual mode (continuous/pulsed) 485nm diode laser (LDH-D-D-485, PicoQuant) was used for exciting the donor, because continuous excitation maximizes the fluorescence emission for a given average excitation power. The emitted fluorescence in each of the two channels passes through an optical wavelength filter (ET525/50m for the donor channel or E600LP for the acceptor channel, Chroma Technology) and is collected by photon-counting avalanche photodiodes (SPCM-AQR-15, PerkinElmer Optoelectronics). The photon arrival time is recorded with 1 ps resolution, and the photodiodes have a response time of about 350 ps.

Two different types of single molecule FRET measurements were performed on the DNA hairpin. In one, the molecule was freely diffusing and produces a burst of photons while in the focal spot of the confocal microscope. In immobilization measurements, the molecule was attached to a polyethylene glycol coated surface via a biotin-streptavidin-biotin linkage as shown in Fig. 2. The free diffusion measurements were employed to determine the salt concentration that would produce comparable populations of folded and unfolded molecules at room temperature. Diffusion limits photon detection to the molecule's brief residence time in the confocal volume (~0.5 ms), whereas the immobilization observation time is limited only by the lifetime of one of the dyes before photobleaching. Immobilization is therefore the preferred method for determining kinetics and average transition path times.

Sample preparation for free diffusion experiments. For free diffusion measurements, 25 μL of a solution of 40 pM VS4T21bio DNA, 500mM NaCl, 20mM Tris-HCl (pH 8.0), 250 μM EDTA, and 0.01% Tween-20 (Thermo Scientific)) was placed on a glass cover slip that had been rinsed with water, methanol, and dried with nitrogen gas. The sample was covered with a CoverWell cell (PCI-0.5, Grace Bio-Labs) to reduce evaporation during the measurement. The surfactant Tween was used to prevent the DNA from sticking to the glass or CoverWell surface. The confocal volume was set to 20 μm above the glass surface, and molecules were detected as they diffused in and out of the focal volume, which is illuminated with a laser intensity of 14 kW/cm^2. The very low concentration (40 pM) of DNA used makes it highly unlikely that two molecules would be in the illuminated volume simultaneously [1]. Data was collected for one hour, divided into 1 ms time bins, and only bins with more photons than a given threshold (e.g. 30 photons/bin) were analyzed (Fig. S2).

Sample preparation and data acquisition for immobilization experiments. For immobilization studies, the biotin-modified DNA hairpins were tethered to a biotin-

embedded, polyethyleneglycol (PEG)-coated glass coverslip (Bio_01, Microsurfaces Inc.) via a biotin (surface)-streptavidin-biotin (DNA) linkage, as illustrated in Fig. 2 (main text). The coverslip was cleaned with DNase-free water and dried with a nitrogen gas stream. An adhesive Coverwell (PC8R-0.5) chamber was attached to the surface to prevent evaporation. Two 2 mm holes in the chamber allow solution to be inserted and removed with a micropipette. In each step a quantity of 20 μL of solution was inserted and then removed. First a streptavidin solution (25 μg/mL) was inserted, allowed to bind to the biotin for 2 minutes, and then replaced with 100mM Tris-HCl pH 8.0 buffer. Next, a 300 pM solution of the biotinylated DNA hairpin in 20mM Tris-HCl was left on the surface for several minutes. The DNA solution was replaced by the measurement buffer, a solution of 500 mM NaCl, 250 μM EDTA, 20 mM Tris-HCl (pH 8.0), 1 mM L-ascorbic acid (A92902, Sigma), and 1 mM methyl viologen (856117, Sigma). The ascorbic acid and methyl viologen were added to minimize both blinking and photobleaching [2]. An additional exchange of the measurement buffer reduces the concentration of non-immobilized DNA molecules present for the measurement.

Automated data collection of immobilization trajectories was performed at room temperature. Initial raster scanning located the immobilized fluorophores with a laser power density of ~0.2 kW/cm^2, while higher power densities of ~2 kW/cm^2 and ~20 kW/cm^2 were used to collect trajectories for the determination of rate coefficients and transition path times, respectively [3].

Data Analysis

Selection of trajectories for analysis. At low intensity (2 kW/cm^2), ~66% of the photon trajectories were not analyzed because they (i) contained only donor photons as a result of acceptor bleaching, (ii) the confocal volume contained 2 molecules, as judged by two-step bleaching of donor or acceptor (iii) the donor spectrum showed a red shift, as judged by a FRET efficiency > 0.12 following acceptor bleaching [4], (iv) the molecule remained in the folded or unfolded state, as identified by the FRET efficiency, for more than ten times the mean expected waiting time in that state, presumably the result of an interaction with the surface (v) the emission arose from impurities, as judged by extremely high or irregular photon count rate, or (vi) acceptor blinking was too frequent, as judged by multiple long strings of donor photons.

For the high intensity measurements (~20 kW/cm^2), we selected only trajectories that contained transitions, retaining ~30% of measured trajectories for analysis. The Viterbi algorithm located the most probable point in each trajectory at which a transition between folded and unfolded states occurred [5, 6]. Sufficiently long segments containing a single transition were then used in for the maximum likelihood analysis.

Calculation of the donor-acceptor cross correlation. The donor-acceptor cross correlation function for the *j*th trajectory is defined as

$$C_{DA}^{j}(\tau) = \frac{\langle N_D(t+\tau)N_A(t)\rangle}{\langle N_D\rangle\langle N_A\rangle} - 1 \qquad \text{(S1)}$$

where $N_D(t)$ and $N_A(t)$ are the number of donor and acceptor photons in a bin at time t, and $\langle\ \rangle$ indicates an average. Fig. S3 plots the average over all 200 C_{DA}^{j} for the low intensity immobilization data.

Details of the transition path time calculation. The average transition path time was determined using the three-state model in Fig. 4A**.** Folded and unfolded segments were identified with the Viterbi algorithm as in Ref. [7] . If multiple transitions were found in a given trajectory, the trajectory was divided into segments with one transition per segment prior to analysis.

The two-state parameters k_F and k_U (from $\mathbf{K}_{2\text{-state}}$), are related to the three-state parameters $k_{F'}$ and $k_{U'}$ (from Eq. 4), by $k_{F'} \approx 2k_F$ and $k_{U'} \approx 2k_U$ (see Supplementary Online Material from Ref. [6]). $k_{F'}$ and $k_{U'}$ were determined by the low intensity immobilization experiment and two-state maximum likelihood analysis. To ensure the analysis of a single transition, all rates were scaled to be slower by a factor of 1000 and the states at the beginning and the end of the segment were fixed to the states already assigned by the Viterbi algorithm. Thus, $k_{F'} \approx k_F / 500$ and $k_{U'} \approx k_U / 500$.

For a trajectory to be included in the analysis, segments before and after the transition were required to be at least 100 μs in duration and have a FRET efficiency within two standard deviations of the mean efficiency of all either unfolded or folded segments. Only ~ 5% of the transitions were rejected due to anomalous FRET efficiencies, due, for example, to the DNA molecule sticking to the surface. About 45% of the transitions were discarded for being too short because of donor or acceptor blinking longer than the 50 μs bintime, which shortened many photon segments near the transitions. The result of the above filtering was that 780 segments containing a single transition were analyzed using the maximum likelihood function.

Effect of acceptor blinking on transition path time analysis. Acceptor blinking interferes with our analysis because the residence time in the non-emitting ("dark") state of the acceptor appears as an additional state with very low FRET efficiency in the trajectories. However, the simplest possible filtering procedure of deleting trajectories that contain strings of 8 or more green photons near the transition (~10% of measured transitions) eliminates the contribution of blinking in our maximum likelihood analysis of the average transition path time. This is demonstrated in Figure S5, where the data is analyzed before and after the deletion, as well with a 6-state kinetic model (Figure S4) that explicitly included the kinetics of acceptor blinking. The comparison between removing the effect of blinking by excluding trajectories with green photon strings or by the more elaborate method of analyzing the data without this filtering with a 6-state model shows that both yield almost identical upper bounds.

Recoloring. A technique called recoloring tests whether a model accurately describes the data [8] . In recoloring, the observed intervals between the photon arrival times are retained, but the photon color is reassigned according to the model parameters (E_U, E_F, k_U, k_F) derived from the maximum likelihood analysis. A FRET efficiency histogram constructed from this new recolored photon trajectory can then be compared to the original histogram. Fig. S2

shows the comparison of histograms from free diffusion and low intensity immobilization photon trajectories that were recolored using the two-state model. The wider, blue histogram bars are the experimental data and the narrow, red bars are the recolored histograms. The near perfect match indicates that the simple two-state model is an adequate description of the data.

To determine the transition path time that could be detected using our data set, the same set of high intensity trajectories (used to produce Figure 4B) were recolored using a three-state model. The data was recolored for six different assumed values of t_{TP}. For each value of t_{TP}, 5 sets of recolored photon trajectories were calculated using the experimental parameters from Table SI. $\Delta \ln L$ was then calculated using the three state model for each set of trajectories and plotted vs τ_S in Figure S6 as was done for the observed data. No significant peaks are observed in $\Delta \ln L$ for $t_{TP} \leq 5$ μs.

	E_F	E_U	k_F (ms^{-1})	k_U (ms^{-1})	Folded fraction
Free diff. (T30)	0.905± 0.001	0.525± 0.001	1.26± 0.10	2.92± 0.10	0.302± 0.004
Immob. (T30)	0.853± 0.001	0.491± 0.001	1.97± 0.06	3.18± 0.06	0.383± 0.003
Immob. (T50)	0.854± 0.001	0.492± 0.001	2.00± 0.06	3.13± 0.06	0.389± 0.003

TABLE SI. FRET efficiencies, *E*, for the folded and unfolded states, rate coefficients, *k*, for the folding and unfolding transitions, and the fraction of molecules that are folded as measured for a DNA hairpin in 500 mM NaCl by free diffusion and immobilization methods at low intensity (2 kW/cm^2). The agreement is comparable to what has been found in previous studies for proteins, indicating that surface immobilization does not have a major effect on either the stability of the hairpin or its folding kinetics. The fraction folded is also similar to what is determined from thermal unfolding experiments for the same DNA sequence without dyes attached and no biotin linker (Fig. S1). T30 and T50 indicate threshold levels of 30 or 50 photons/bin. For comparison, fluorescence studies by Narayanan *et al*. measured the same DNA hairpin labeled with FAM and Alexa Fluor 647 and no biotin linker to be around 70% folded at the temperature of our measurements (22º C)[9]. Temperature jump and rapid mixing experiments gave relaxation rates of about 10 ms^{-1} and 5 ms^{-1}, respectively [9]. The stability difference must be attributed to the different dyes, but given that different dyes were used, the relaxation rate compares well with the sum of folding and unfolding rates reported here. Different measurements have shown possible evidence for a three-state mechanism under conditions that differ from the ones reported here. Kugel *et al.* observed FCS data from a DNA hairpin similar to the one discussed here that deviates from a two state model for certain fluorophores while other fluorophores produce two state data for the same DNA hairpin [11]. Jung *et al*. also previously measured the hairpin discussed here using a rhodamine-dabcyl quenching system and reported the presence of a metastable intermediate [10]. However, their labeled hairpin was much more stable than found in our study and that of Narayanan et al., and all of the measurements of Jung et al were made in 100 mM NaCl while our measurements are at 500 mM NaCl. Narayanan *et al*. saw some hints of biexponential kinetics at 100 mM NaCl, but all other measurements, including those at 500 mM, were clearly two-state [9]. Finally, if there were an observable kinetic intermediate with the rates described by Jung et al., it would appear as a peak in our three-state likelihood calculations. No such peak is observed.

E_F	0.852 (±0.0009)
E_U	0.498 (±0.0009)
k_b (ms^{-1})	309 (±9)
p_b at a photon count rate of 100 ms^{-1}	0.995 (±0.0001)

TABLE SII. Maximum likelihood parameters from the 6-state transition path time analysis. Standard deviations given are the diagonal terms of the covariance matrix calculated from the likelihood function.

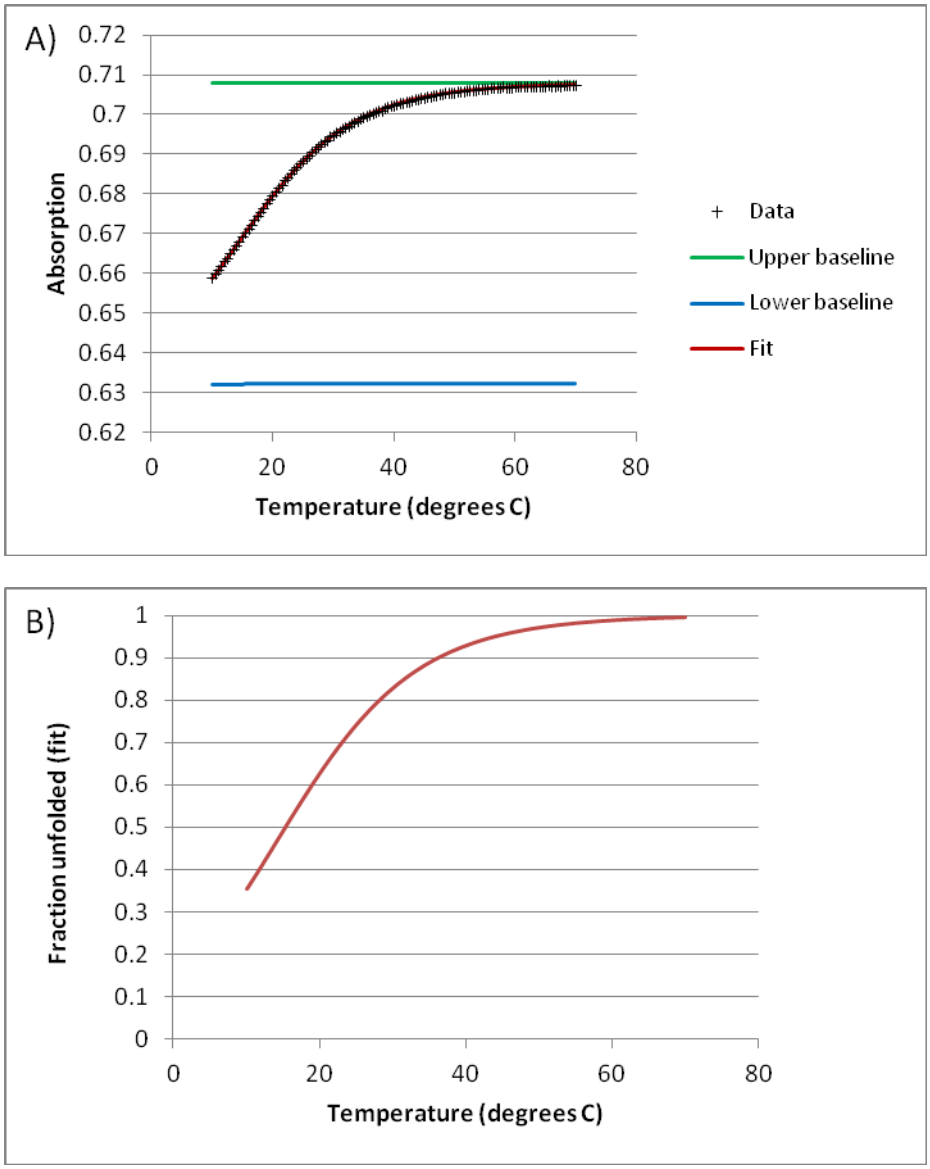

FIG. S1. (a) Data (black line) from an equilibrium absorption melt of the DNA hairpin sequence AACC -(T_{21})-GGTT without biotin, linkers or dyes in a solution of 3 µM DNA, 500 mM NaCl, 250 µM EDTA, and 2.5 mM Tris-HCl (pH 8.0). The curve is a fit to a two-state van't Hoff transition with linear baselines. Since the lower baseline is not observed, it is assumed to be parallel to the upper baseline. (b) Fraction folded based on the two-state fit.

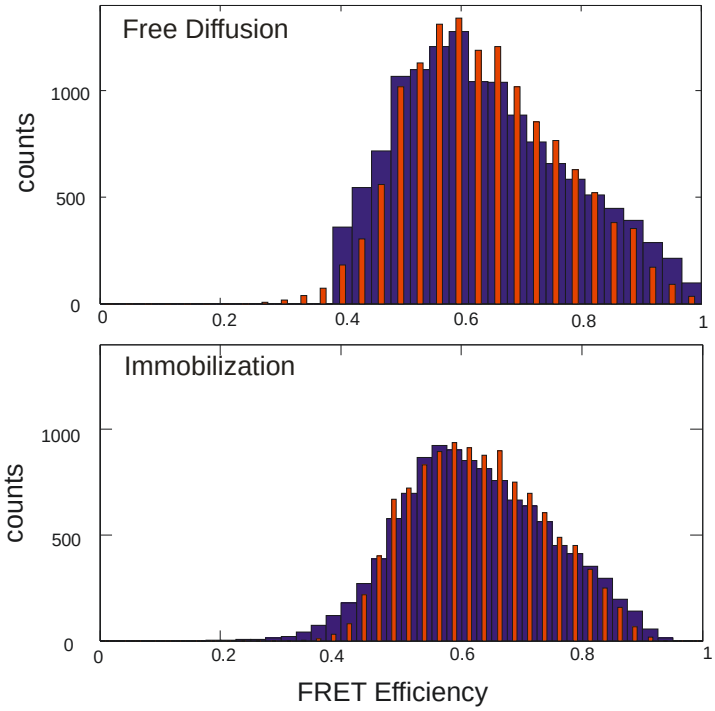

FIG. S2. FRET efficiency histograms calculated from 1 ms bins for data (wide, blue bars) and recolored histograms (thin, red bars). A threshold of 30 photons/bin was applied for both data sets. For the free diffusion data, FRET efficiencies below 0.4 are omitted to suppress the donor only peak. Similarly, segments of the immobilization trajectories that are categorized as donor only are omitted. Only segments that pass the filtering criteria described in the supplementary information are plotted. The immobilization data was collected at the lower intensity of 2 kW/cm^2.

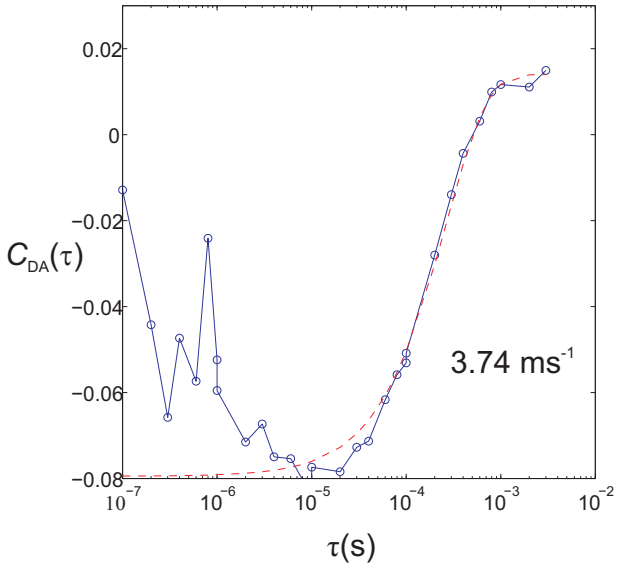

FIG. S3. Donor-acceptor cross-correlation function (Eq. S1) calculated from low power density (2 kW/cm^2) immobilization data. The red dashed line is an exponential fit to the cross-correlation over the range 2 μs to 3 ms, from which a decay time of 3.74 ms^{-1} was extracted. This decay time can be compared to the sum of the folding and unfolding times found by the maximum likelihood method.

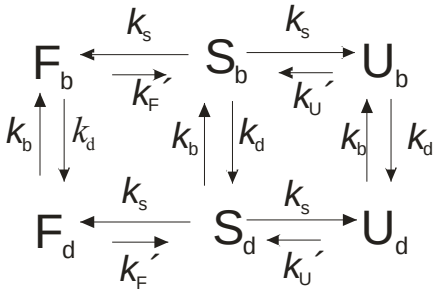

FIG. S4. Six state model including acceptor blinking. F, S, and U indicate the folded, intermediate, and unfolded states. Subscripts b and d indicate the bright and dark states of the acceptor, respectively.

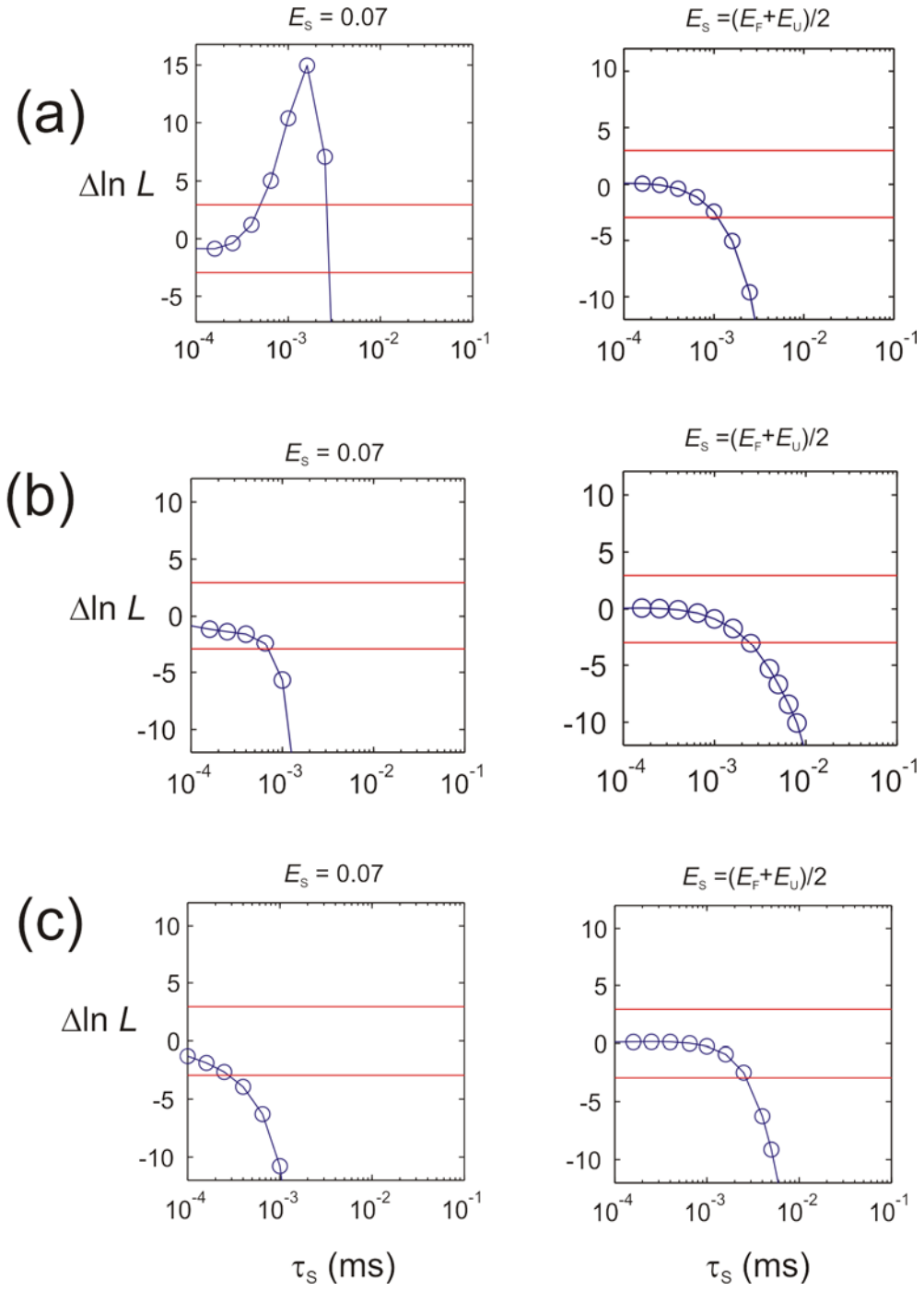

FIG. S5. Effect of acceptor blinking. In the left column the data is analyzed assuming an intermediate state FRET efficiency of E_S=0.07, corresponding to the dark state of the acceptor (It is not 0 because there is leakage of donor photons into the acceptor channel). In the right column the data is analyzed with an intermediate FRET efficiency of $E_S = (E_F + E_U)/2$). For rows (a) and (b) a three state model was used to calculate the likelihood function. In (a) no acceptor blinking filtering was used. In row (b) transitions with acceptor blinking (defined by a string of 8 or more donor photons) within 30 μs of the transition were

excluded from the analysis. (c) The six-state model shown in Fig. S4 was used to calculate the likelihood function, and no acceptor blinking filtering was used. In this model there are fluorescing ("bright") and non-fluorescing ("dark") versions of each state. The assumptions of the model are that the residence time in all states is an exponential distribution [12, 13], the kinetic rates among the bright states are the same as among the dark states, the transition rate from a bright to a dark state (k_d) is proportional to the photon count rate in a given trajectory, and the transition rate from a dark to a bright state (k_b) is independent of the photon count rate. The fractional population in the bright acceptor state is defined as ($p_b = k_b/[k_b + k_d]$). The rate matrix in the likelihood function for this model is

$$\mathbf{K}_{\text{6-state}} = \begin{pmatrix} -k_{U'} - k_d & k_S & 0 & k_b & 0 & 0 \\ k_{U'} & -2k_S - k_d & k_{F'} & 0 & k_b & 0 \\ 0 & k_S & -k_{F'} - k_d & 0 & 0 & k_b \\ k_d & 0 & 0 & -k_{U'} - k_b & k_S & 0 \\ 0 & k_d & 0 & k_{U'} & -2k_S - k_b & k_{F'} \\ 0 & 0 & k_d & 0 & k_S & -k_{F'} - k_b \end{pmatrix},$$

$\mathbf{v}_{ini} = [0\ 0\ p_b\ 0\ 0\ (1 - p_b)]^{\mathrm{T}}$, and $\mathbf{v}_{fin} = [1\ 0\ 0\ 1\ 0\ 0]^{\mathrm{T}}$ for the six-state model. The quantity $\Delta \ln L(0)$ is maximized by varying k_b, k_d, E_{F}, and E_{U}. These optimized values, shown in Table SII, are then used to calculate $\Delta \ln L(\tau_{\mathrm{TP}})$. The red lines have the same meaning as in Fig. 4B of the main text.

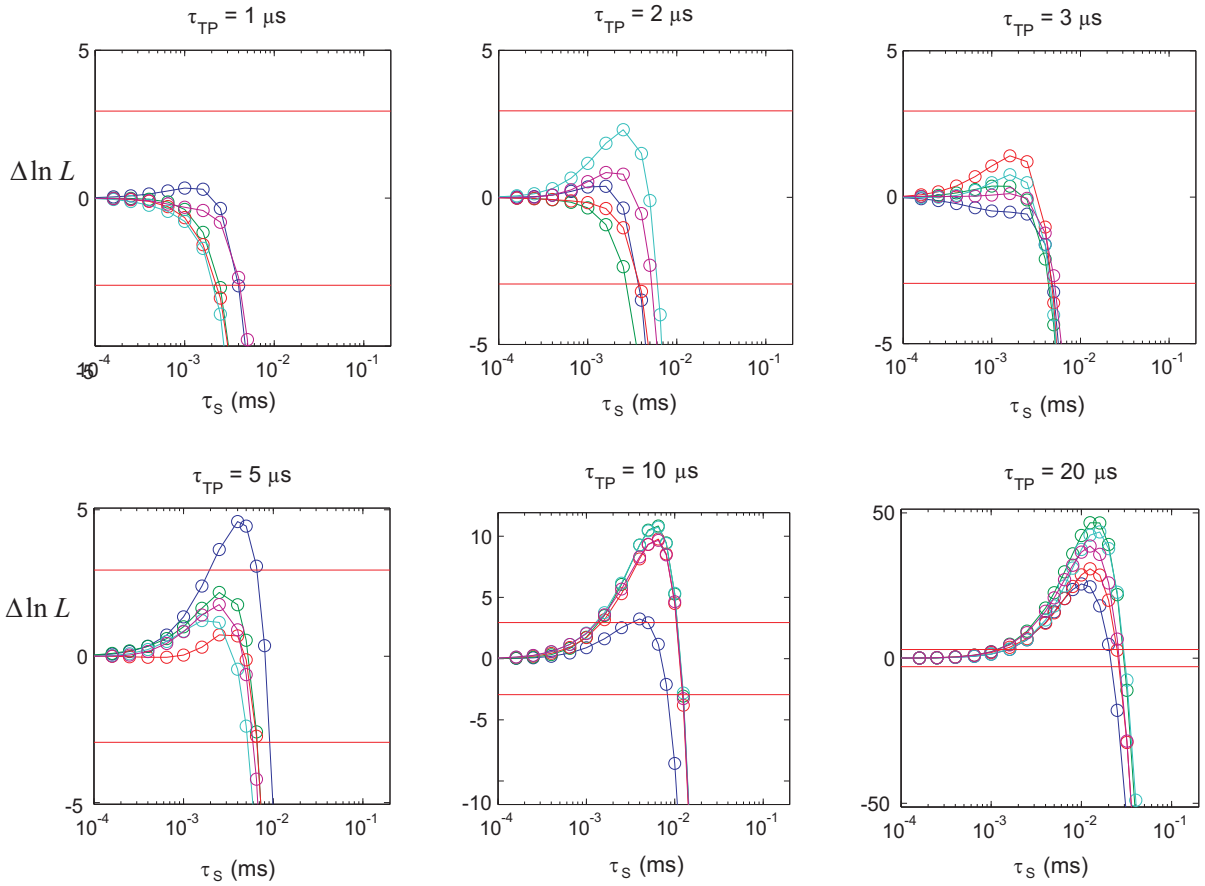

FIG. S6. Plots of Δln L, the difference in the natural logarithm of the likelihood function, for the data from Fig. 4B recolored with the three-state model. Trajectories with acceptor blinking were excluded. The red lines have the same meaning as in Fig. 4B. Each plot contains five independent recoloring simulations.

References

[1] I. V. Gopich, Concentration effects in "single-molecule" spectroscopy. J. Phys. Chem. B **112**, 6214 (2008).

[2] J. Vogelsang, R. Kasper, C. Steinhauer, B. Person, M. Heilemann, M. Sauer, and P. Tinnefeld, A reducing and oxidizing system minimizes photobleaching and blinking of fluorescent dyes. Angew.Chem. **47**, 5465 (2008).

[3] H. S. Chung, K. McHale, J. M. Louis, and W. A. Eaton, Single-molecule fluorescence experiments determine protein folding transition path times. Science **335**, 981 (2012).

[4] H. S. Chung, J. M. Louis, and W. A. Eaton, Experimental determination of upper bound for transition path times in protein folding from single-molecule photon-by-photon trajectories. Proc. Natl. Acad. Sci. USA **106**, 11837 (2009).

[5] L. R. Rabiner, A tutorial on hidden Markov models and selected applications in speech. Proc. IEEE **77**, 257 (1989).

[6] A. J. Viterbi, Error bounds for convolution codes and an asymptotically optimum decoding algorithm. IEEE Trans. Information Theory **13**, 260 (1967).

[7] H. S. Chung, I. V. Gopich, K. McHale, T. Cellmer, J. M. Louis, and W. A. Eaton, Extracting rate coefficients from single-molecule photon trajectories and FRET efficiency histograms for a fast-folding protein. J. Phys. Chem. A **115**, 3642 (2011).

[8] I. V. Gopich, and A. Szabo, Decoding the pattern of photon colors in single-molecule FRET. J. Phys. Chem. B **113**, 10965 (2009).

[9] R. Narayanan, L. Zhu, Y. Velmurugu, J. Roca, S. V. Kuznetsov, G. Prehna, L. J. Lapidus, and A. Ansari, Exploring the energy landscape of nucleic acid hairpins using laser temperature-jump and microfluidic mixing. J. Am. Chem. Soc. **134**, 18952 (2012).

[10] J. Jung, R. Ihly, E. Scott, M. Yu, and A. Van Orden, Probing the complete folding trajectory of a DNA hairpin using dual beam fluorescence fluctuation spectroscopy. J. Phys. Chem. B **112**, 127 (2008).

[11] W. Kugel, A. Muschielok, and J. Michaelis, Bayesian-Inference-Based Fluorescence Correlation Spectroscopy and Single-Molecule Burst Analysis Reveal the Influence of Dye Selection on DNA Hairpin Dynamics. Chemphyschem **13**, 1013 (2012).

[12] M. Orrit, Chemical and physical aspects of charge transfer in the fluorescence intermittency of single molecules and quantum dots. Photochem. Photobiol. Sci. **9**, 637 (2010).

[13] T. Cordes, J. Vogelsang, and P. Tinnefeld, On the Mechanism of Trolox as Antiblinking and Antibleaching Reagent. J. Amer. Chem. Soc. **131**, 5018 (2009).